Lawrence Berkeley National Laboratory

Recent Work

Title

Thermoelectric Properties of Poly(3-hexylthiophene) (P3HT) Doped with 2,3,5,6-Tetrafluoro-7,7,8,8-tetracyanoquinodimethane (F4TCNQ) by Vapor-Phase Infiltration

Permalink

https://escholarship.org/uc/item/35b760w4

Journal

Chemistry of Materials, 30(3)

ISSN

0897-4756

Authors

Lim, E
Peterson, KA
Su, GM
et al.

Publication Date

2018-02-13

DOI

10.1021/acs.chemmater.7b04849

Peer reviewed

eScholarship.org Powered by the California Digital Library
University of California

This is an open access article published under an ACS AuthorChoice License, which permits copying and redistribution of the article or any adaptations for non-commercial purposes.

CHEMISTRY OF MATERIALS
Cite This: Chem. Mater. 2018, 30, 998−1010
Article
pubs.acs.org/cm

Thermoelectric Properties of Poly(3-hexylthiophene) (P3HT) Doped with 2,3,5,6-Tetrafluoro-7,7,8,8-tetracyanoquinodimethane (F_4TCNQ) by Vapor-Phase Infiltration

Eunhee Lim,[†] Kelly A. Peterson,[†] Gregory M. Su,[‡] and Michael L. Chabinyc*,[†]

[†]Materials Department, University of California, Santa Barbara, California 93106, United States
[‡]Advanced Light Source, Lawrence Berkeley National Laboratory, Berkeley, California 94720, United States

Supporting Information

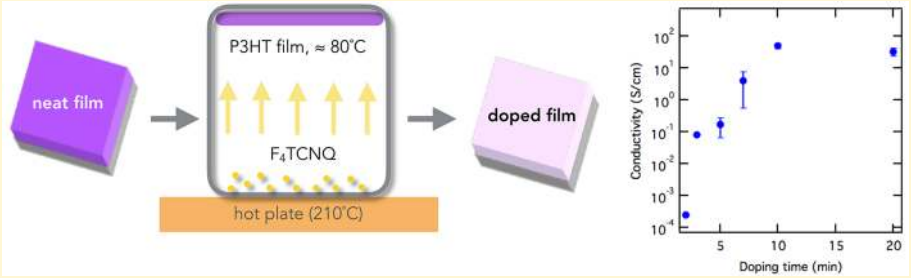

ABSTRACT: Doping of thin films of semiconducting polymers provides control of their electrical conductivity and thermopower. The electrical conductivity of semiconducting polymers rises nonlinearly with the carrier concentration, and there is a lack of understanding of the detailed factors that lead to this behavior. We report a study of the morphological effects of doping on the electrical conductivity of poly(3-hexylthiophene) (P3HT) thin films doped with small molecule 2,3,5,6-tetrafluoro-7,7,8,8-tetracyanoquinodimethane (F_4TCNQ). Resonant soft X-ray scattering shows that the morphology of films of P3HT is not strongly changed by infiltration of F_4TCNQ from the vapor phase. We show that the local ordering of P3HT, the texture and form factor of crystallites, and the long-range connectivity of crystalline domains contribute to the electrical conductivity in thin films. The thermopower of films of P3HT doped with F_4TCNQ from the vapor phase is not strongly enhanced relative to films doped from solution, but the electrical conductivity is significantly higher, improving the thermoelectric power factor.

INTRODUCTION

The ability to control the electrical conductivity of organic semiconductors is desirable for tuning the performance of organic electronic devices. For example, the electrical conductivity and Fermi level of electrode layers in organic solar cells and organic light emitting diodes play an important role in efficient charge extraction and injection in the device.[1−4] Electrical doping is of paramount importance for thermoelectric devices where the carrier concentration impacts all of the factors—the electrical conductivity, σ, the thermal conductivity, κ, and the Seebeck coefficient, S—in the figure of merit, $ZT = S^2\sigma T/\kappa$.[5−7] Despite significant progress in understanding structure−property relationships in semiconducting polymers, it is still not well understood how electrical conductivity is related to doping, particularly as a function of processing method.[8]

Here we examine how differences in the processing method of a common *p*-type dopant change the electrical properties of poly(3-hexylthiophene) (P3HT). We show how introduction of the molecular dopant F_4TCNQ from the vapor phase impacts the microstructure of thin films of P3HT and the resulting electrical conductivity. Our results demonstrate that processing has a significant influence on electrical conductivity and that vapor-phase doping provides a pathway to understand the role of morphology on charge transport.

Electrical conductivity is not a simple function of charge concentration in semiconducting polymers due to their energetic and structural disorder.[8] Introduction of charge carriers can be achieved when a dopant molecule with appropriate electronic levels is added to a host polymer. For *p*-type doping, adding a molecule whose electron affinity is offset to be below the ionization energy of the organic semiconductor allows electron transfer between the two molecules, thus creating charged species. The increase in charge carrier density leads to an increase in the electrical conductivity. For solution-processed materials, if the dopant is added to a solution of the polymer, charge transfer can lead to aggregation of the polymer (and dopant) in solution and strongly modify the morphology of the resulting solid film.[9−11]

Received: November 18, 2017
Revised: December 24, 2017
Published: January 29, 2018

© 2018 American Chemical Society

DOI: 10.1021/acs.chemmater.7b04849
Chem. Mater. 2018, 30, 998−1010

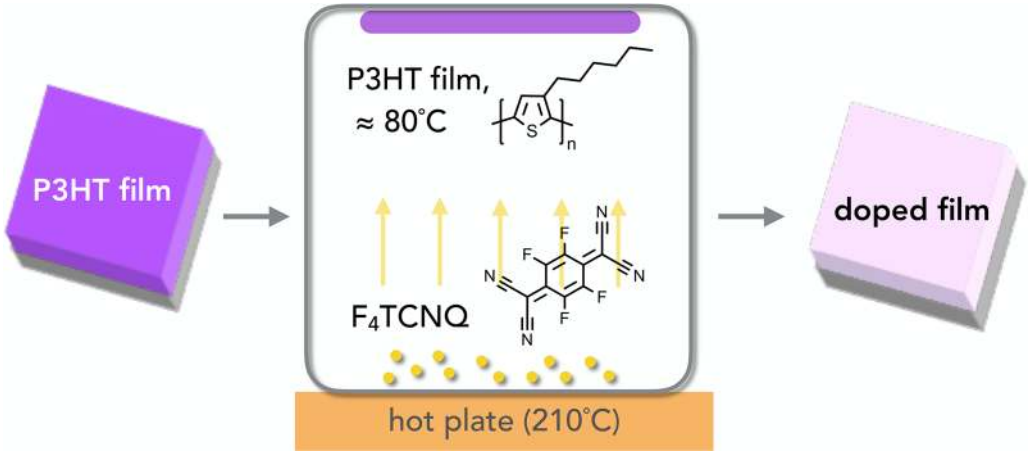

Figure 1. Schematic of vapor-doping method used in this study. The height of the doping chamber is 5 cm. The chemical structures of P3HT and F_4TCNQ are shown.

A nonlinear change in conductivity with the dopant concentration has been observed in many systems. For example, with an increase in dopant concentration in P3HT doped with 2,3,5,6-tetrafluoro-7,7,8,8-tetracyanoquinodimethane (F_4TCNQ), a decrease in conductivity is observed over a small range at ultralow[12] and high[13] doping levels followed by a linear and nonlinear increase at moderate doping levels,[9] which has been attributed to filling of electronic trap states.[13,14] The electrical conductivity of films with the same dopant concentration can vary dramatically depending on the doping methods used.[15] It is therefore difficult to attribute changes in electrical properties solely due to changes in the charge carrier concentration.

There has been significant work to try to understand the role of processing on electrical conductivity using P3HT and the charge transfer dopant F_4TCNQ as a model system. P3HT is a well-studied semiconducting polymer whose crystal structure and optical and electrical properties of neat thin film are known. In the case of solution doping, the polymer and dopant are mixed and then cast into a solid film.[11,13,16−20] In contrast, using sequential doping the neat polymer film is cast and the dopant is deposited from an orthogonal solvent on the neat polymer film.[9,21,22] Sequentially doped films have been shown to have higher conductivity than that of solution doped samples at the same dopant concentration. These differences have been attributed to a smaller perturbation in the microstructure of the film during sequential casting thereby allowing tie-chains connecting crystalline domains formed in neat P3HT to be retained leading to high conductivity.[22] On the other hand, in solution doping, P3HT:F_4TCNQ aggregates form due to charge transfer in solution causing a different morphology in the cast films with poorly connected domains. With the same dopant concentration, solvents with different polarity have been shown to cause over an order of magnitude difference in conductivity due to changes in aggregation.[20] Post-processing to increase the conductivity, such as thermal annealing, is difficult with P3HT:F_4TCNQ films because the dopants can decompose or be removed from the film at elevated temperatures. Some groups have tried aligning the polymer backbone in neat films and then infiltrating the dopants to the aligned film. Stretch-aligned P3HT films doped with F_4TCNQ by vacuum evaporation showed 2−3 times higher mobility and conductivity compared to pristine films.[23] About 7 times higher conductivity was reported for films aligned by high-temperature rubbing and doped by sequential casting compared to that of nonaligned films.[7]

Recently, it has been shown that F_4TCNQ can be introduced into semiconducting polymers from the vapor phase.[15,24−27] Solid-state diffusion of F_4TCNQ into PBTTT leads to a 100-fold increase in conductivity compared to solution doped films.[15,26] This difference was attributed to retention of the microstructure during vapor doping.[15,26] The high conductivity was further correlated to the long-range orientational correlation length (OCL) of domains measured using resonant soft X-ray scattering (RSoXS). Mixing the dopant and polymer in solution was found to lead to short OCLs in PBTTT:F_4TCNQ films while solid-state diffusion retains the longer OCL of the neat PBTTT film in the doped form. Whether the morphology of neat-cast films of other polymers is retained during vapor infiltration of F_4TCNQ is currently not known.

Here, we study how the introduction of F_4TCNQ from the vapor phase affects the morphology and electrical conductivity of P3HT films. Doped films are prepared by allowing sublimated F_4TCNQ to diffuse into the neat P3HT film (Figure 1). We find that vapor does not strongly modify the morphology of P3HT from the as-cast film using a combination of grazing incidence wide angle X-ray scattering (GIWAXS) and resonant soft X-ray scattering (RSoXS). The morphological evolution of vapor-doped films, combined with optical and electrical measurements, shows that vapor infiltration at mild temperatures leads to efficient doping and that the texture and length of fibrils in ordered domains dictate the conductivity at high carrier concentration.

RESULTS AND DISCUSSION

Optical Absorption Spectra Show Charge Transfer via Solid-State Diffusion. Vapor infiltration of F_4TCNQ into polymer thin films can be readily accomplished. The volatility of F_4TCNQ allows deposition under vacuum where the mass of material deposited can be measured using a quartz crystal microbalance. However, F_4TCNQ can also be sublimed readily at atmospheric pressure allowing simpler methods to be used. Here vapor doping was carried out in a custom doping vessel (≈0.4 L) in a nitrogen glovebox, and the charge concentration was determined after doping using spectroscopic methods. Because of the question of how the dopant infiltrates the polymer at a given deposition temperature, there is no

DOI: 10.1021/acs.chemmater.7b04849
Chem. Mater. 2018, 30, 998−1010

particular disadvantage for using atmospheric pressure deposition and determining the concentration in the bulk after doping.

The interpretation of measurements of electrical conductivity as a function of processing method requires knowledge of the charge carrier concentration. Optical absorption spectroscopy provides a means to determine the extent of charge transfer between P3HT and F_4TCNQ in vapor-doped film from the characteristic features of their neutral and charged forms.[12] Figure 2 shows optical spectra of P3HT films doped with

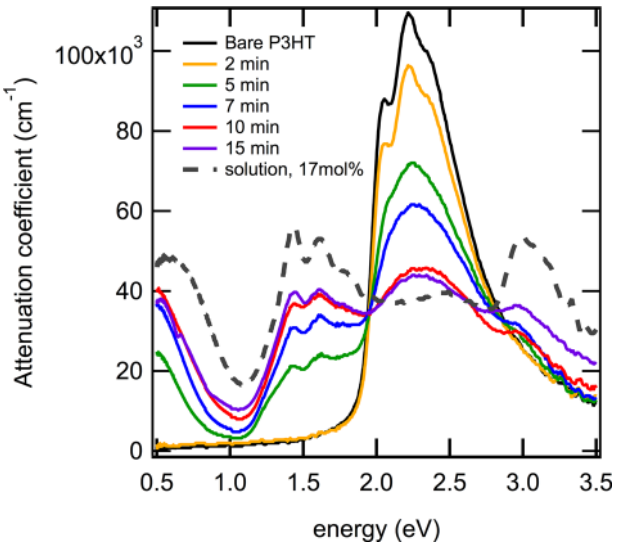

Figure 2. Optical absorption spectra of P3HT films vapor-doped with F_4TNCQ for various times and a 17 mol % solution-doped film.

F_4TCNQ vapor for varying amounts of time. After 5 min of exposure to a vapor of F_4TCNQ under our conditions, a peak near 0.5 eV assigned to the polaron of P3HT and peaks near 1.4 and 1.6 eV assigned to the anion of F_4TCNQ appear. These features are indicative of integer charge transfer between P3HT and F_4TCNQ.[28] With increased doping time, the intensity of these peaks increases and intensity of features assigned to the neutral form of P3HT around 2.3 eV decreases. The dopant composition increased linearly with time between 5 and 10 min, where it saturated based on the absorbance spectra.

The dopant concentrations in films were determined with the optical spectra using two different fitting methods, and the estimated concentrations from the two methods are in a reasonable agreement. The first method is to use the ratio of the neutral and polaron peaks of P3HT as a function of the concentration of F_4TCNQ. This method has been used to compare the concentration in films doped by sequential casting from solvent to solution doped films with known dopant concentrations (Figure S1).[22] For our vapor-doped P3HT films the P3HT polaron peak at 0.5 eV is well-isolated from other peaks, but there is an uncertainty in the fitting of the spectral features of neutral P3HT due to a change in the shape as a function of doping. The second method relies on the integrated intensity of the absorption of the anion of F_4TCNQ and P3HT neutral peak using Beer's law and known attenuation coefficients. Because the features of F_4TCNQ overlap with the polaron feature of P3HT near 1.5 eV, this method also has some uncertainly. Recent measurements of the polarized optical spectra of aligned P3HT film doped with F_4TNCQ revealed that the polymer backbone and the π-face of the dopant are oriented perpendicular to each other in the film.[29] This measurement separates the absorption of P3HT and F_4TCNQ allowing the concentration of the F_4TCNQ anion to be estimated using a molar extinction coefficient of $\varepsilon \approx 50\,000$ L mol^{-1} cm^{-1} (Figure S2).[12] Because neat P3HT films were initially cast from solutions with the same concentration of P3HT, the thickness was taken to be identical and the total P3HT concentration was calculated using the peak around 2.3 eV with a molar extinction coefficient of $\varepsilon \approx 10\,000$ L mol^{-1} cm^{-1}.

The two methods provide good agreement in estimated dopant concentration in vapor-doped films. Table 1 summarizes the estimated F_4TCNQ concentrations in vapor-doped samples, in units of mol % F_4TCNQ per monomer of P3HT. Concentrations from two methods agree within 2 mol %. The slightly lower concentration of F_4TCNQ using anion peak fitting for saturation-doped samples could be due to the rapid increase of a neutral form of F_4TCNQ near 3.2 eV at high dopant concentration in the film that was not accounted for in this model fitting method. The doping level plateaus after 10 min at ≈10 mol % F_4TCNQ, which corresponds to one F_4TCNQ molecule per 10 P3HT monomers. This result is in a good agreement of the dopant concentration at plateau of the electrical conductivity in sequentially doped films.[22] Reports in the literature on solution-doped samples suggest that maximum conductivity of 8 S/cm occurs at 17 mol % F_4TCNQ, which is about twice the maximum dopant concentration achieved using sequential and vapor doping methods (Table S1).

Table 1. Estimated Dopant Concentrations of Films Vapor-Doped for Varying Amounts of Time Using Two Different Methods

sample	dopant concentration[a] (F_4TCNQ:P3HT monomer mol %)	
neat P3HT	0	0
2 min	0.23 ± 0.3	0
5 min	4.2 ± 0.7	4.5 ± 0.5
7 min	5.5 ± 0.8	6.5 ± 0.6
10 min	9.7 ± 0.1	7.7 ± 0.8
15 min	9.4 ± 0.1	8.4 ± 0.8

[a](left) Using ratio of neutral and polaron P3HT peaks. The ratios from vapor-doped films were compared to those of solution doped films prepared with known concentrations.[9] (right) Using integrated intensity of F_4TCNQ anion and neutral P3HT peaks. Beer's law with known attenuation coefficients was used to calculate the concentrations of F_4TCNQ anion and neutral P3HT.

Because of the uncertainty in the carrier concentration using optical spectroscopy, it is helpful to consider how the absorption of the neutral form of P3HT changes upon doping. The optical gap of P3HT is related to the conjugation length along the backbone, which is estimated to be approximately 20 monomer units in P3HT.[30,31] Formation of charge on the backbone of P3HT result in new states that have a lower optical excitation,[32−34] with a likely differing spatial extent. For example, the comparable extent of polarons in poly(3-dodecylthiophene) is 8.7 thiophene units for positive polarons.[35] Our saturation-doped samples showed a nearly 50% decrease in the absorption of neutral P3HT, indicating that roughly half of the units contributing to the absorption are influenced by the addition of dopants. This is in qualitative agreement with our estimated dopant concentration of one F_4TCNQ molecule for 10 P3HT monomers in most heavily

DOI: 10.1021/acs.chemmater.7b04849
Chem. Mater. 2018, 30, 998−1010

doped films and points out the difficulty of extracting a quantitative carrier concentration using optical spectra.

At high polaron concentration, formation of bipolarons can be favored over polarons, which has been suggested as lower energy charge-storage configuration in solution state.[36] Spectral features around 0.35, 1.3, and 1.6 eV have been assigned to P3HT bipolarons,[18,37] and coexistence of polarons and bipolarons in heavily doped P3HT:F_4TCNQ films have been proposed, but not quantified. In our system, we cannot make a detailed assessment of bipolaron formation due to overlap of the spectral features.

Electrical Conductivity of Vapor-Doped P3HT Films Is Higher than That of Solution-Doped Films. We observe significantly higher maximum conductivity in P3HT films doped by vapor doping than in films doped by other doping methods. Figure 3a shows the in-plane conductivity of doped P3HT films as a function of vapor doping time and dopant concentration. After 3 min of doping, an increase in conductivity was observed which plateaued after 10 min (10 mol %) at 48 S/cm. In our saturation solution doped film, measured conductivity was 2.3 S/cm, which is in a reasonable agreement with maximum conductivity values reported in other groups. With sequential doping method, 5.5 S/cm was reported for spin coated film[38] and 22 S/cm for films aligned by rubbing.[29] To the best of our knowledge, this is one of the highest conductivities measured for P3HT:F_4TCNQ. Additionally, at a comparable dopant concentration, vapor-doping method leads to higher conductivity than solution and sequential doping methods. In films with dopant concentration of about 10 mol %, approximately 1 S/cm was reported for solution-doped films,[19] and 3 S/cm[22] for sequentially doped films. Thus, vapor-doping has 48 and 16 times higher conductivity compared to films at equivalent dopant concentration, prepared by solution and sequential doping methods, respectively.

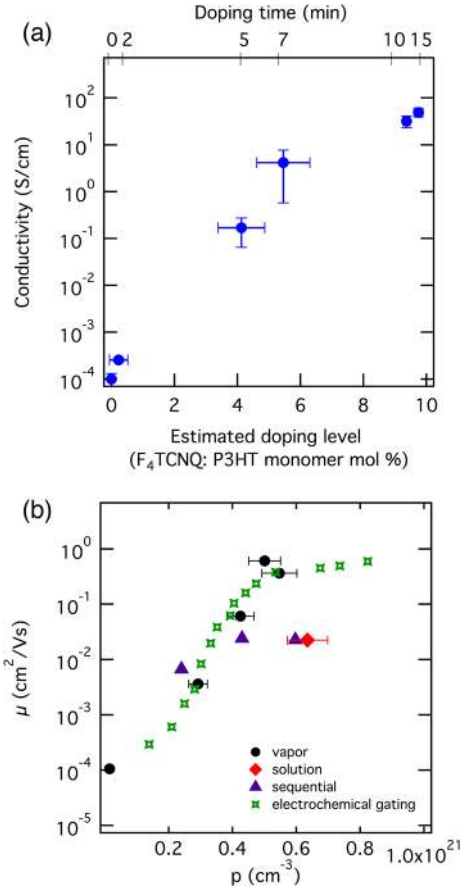

Figure 3. (a) Conductivity of P3HT films doped with F_4TCNQ via vapor doping method for varied amounts of times. The estimated doping level is number of F_4TCNQ monomers per P3HT monomer calculated from fits of the optical spectra. (b) Mobility as a function of carrier concentration. Vapor- and solution-doped films are from this study. Sequential doping [ref 9] and electrochemical gating [ref 39] data are from literature. For the latter, the mobility and charge carrier concentration were measured in an electrochemically gated transistor.

The difference in conductivities at the same doping level can suggest a difference in the mobility of the charged species at the macroscopic scale.[12] The carrier mobility estimated using the carrier concentration determined by optical spectroscopy results in 0.6 $cm^2\ V^{-1}\ s^{-1}$ at carrier concentration of P3HT of $5 \times 10^{20}\ cm^{-3}$ in saturation vapor-doped film (Figure 3(b)). For comparison, electrochemical gating shows mobility of 0.4 $cm^2\ V^{-1}\ s^{-1}$ at similar carrier concentration.[39] The rapid increase in mobility in carrier concentration range in $\sim 10^{20}\ cm^{-3}$ and plateau in the mobility around 0.6 $cm^2\ V^{-1}\ s^{-1}$ are almost identical in vapor-doped and electrochemically gated films. The hole mobility in the saturation solution-doped film is around 0.02 $cm^2\ V^{-1}\ s^{-1}$ with a carrier concentration of $6 \times 10^{20}\ cm^{-3}$, which is consistent with the reported value for sequentially doped films at similar carrier concentrations, determined from Hall coefficient measurements.[9]

The difference in the highest values of the electrical conductivity of solution and vapor-doped films depends on both the carrier mobility and the carrier concentration. Vapor-doped films at the highest concentration of F_4TCNQ were ≈20 times more conductive with ≈30 times higher mobility than the solution doped films that had 120% of the carrier concentration based on optical spectroscopy. The carrier mobility therefore dominates the contribution of the increase in carrier concentration leading to higher conductivity for vapor-doped films of P3HT. In PBTTT:F_4TCNQ films, the main difference between solution and vapor-doped films at comparable carrier concentrations was the charge carrier mobility, which was attributed to the difference in the long-range connectivity of PBTTT crystallites. The increase in conductivity from solid state diffusion in the P3HT:F_4TCNQ (2 S/cm to 48 S/cm) system is not as high as it is in PBTTT:F_4TCNQ, which exhibited more than 100-fold increase from ≈2 S/cm in solution doped films to ≈200 S/cm in vapor-doped films. While it is difficult to compare the two materials directly due to differences in backbone structure, they both show highly efficient charge transfer with F_4TCNQ suggesting that morphological factors such as the fractional crystallinity and texture of domains likely plays a key role in the changes for each system. Thus, an important question is how different the local and longer-range order is in films of P3HT doped from solution and from the vapor phase.

Without knowledge of the domain boundaries and overall morphology, it is difficult to make conclusive remarks on impact of doping ratio and charge mobility. Many studies on solution-doped films have reported a slight dip in mobility at low dopant concentration ($<10^{-3}$ mol %) and superlinear increase in mobility at higher dopant concentrations.[12,40] Numerical and analytic model studies on solution doped films attribute the dip to Coulombic interaction of anions counteracting the filling of trap states and superlinear increase

DOI: 10.1021/acs.chemmater.7b04849
Chem. Mater. 2018, 30, 998−1010

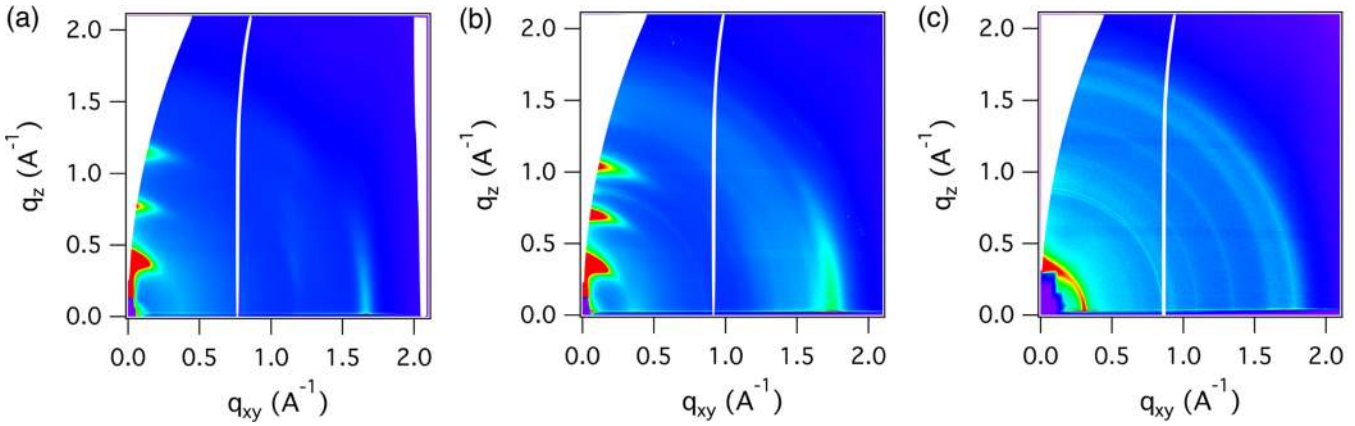

Figure 4. 2D GIWAXS images of (a) neat P3HT, (b) 10 min vapor-doped, and (c) 17 mol % solution doped film.

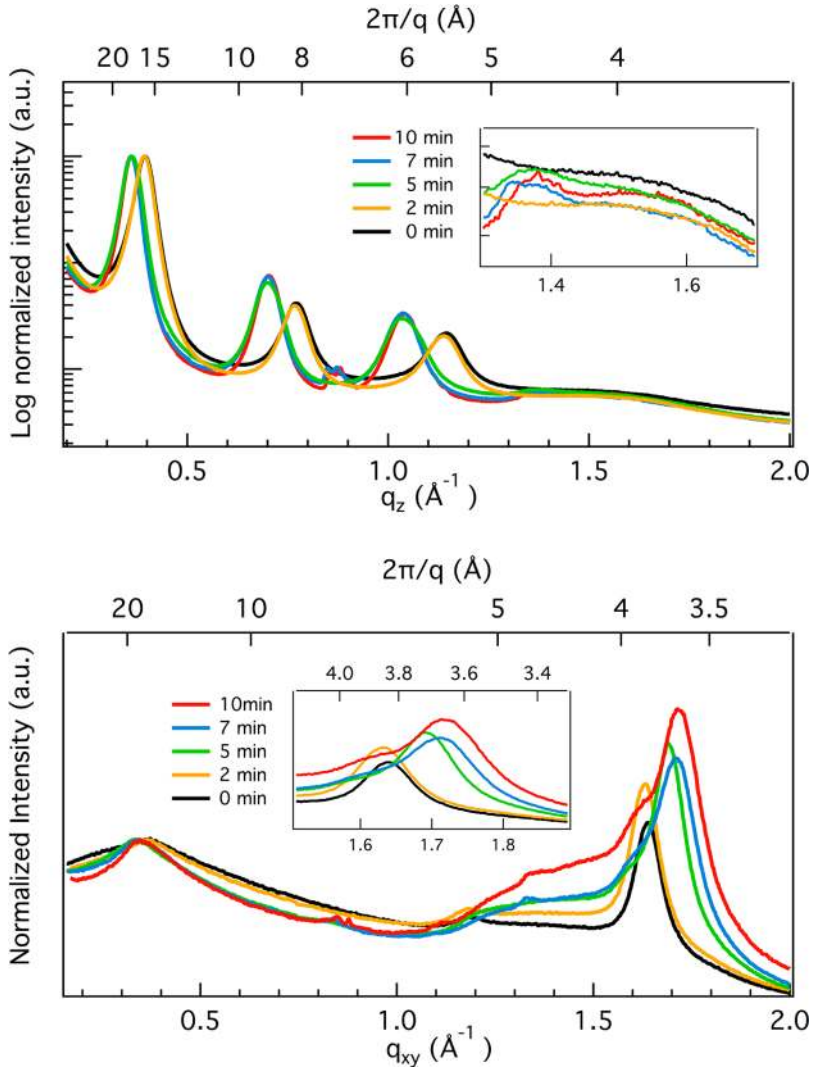

Figure 5. 1D GIWAXS (top) out-of-plane and (bottom) in-plane linecuts along the q_z and q_{xy} direction of P3HT thin films vapor doped with F_4TCNQ for 0 to 10 min.

in mobility solely to the filling of trap states.[40,41] However, evolution of the local structure and the film morphology with increased doping levels has been observed in many recent solution doping studies.[42,13,43,38]

Vapor Doping Preserves the Texture and Modifies the Packing Structure of P3HT. We examined the local structure of films of P3HT doped by F_4TCNQ vapor to determine the changes in local structure using grazing incidence wide angle X-ray scattering (GIWAXS). X-ray scattering from the neat P3HT film suggests preferentially edge-on texture of the crystals, where alkyl stacking is in the out-of-plane direction and $\pi-\pi$ stacking is in the in-plane direction (Figure 4). The

DOI: 10.1021/acs.chemmater.7b04849
Chem. Mater. 2018, 30, 998−1010

alkyl stacking and $\pi-\pi$ stacking distances of neat P3HT are 16.2 and 3.83 Å, similar to previously reported values.[13] Upon doping, preferentially edge-on conformation and the layered texture remain. At doping times of 5 min and longer, the alkyl stacking distance increases from 16.4 to 17.9 Å, and two peaks appear in the region where the neat P3HT $\pi-\pi$ stacking peak was. In the 10 min (Figure 5) doped sample, the two peaks have *d*-spacing values of 3.64 and 3.89 Å. The smaller *d*-spacing has been assigned to the π stacking distance, whereas the larger *d*-spacing is from the cocrystal of P3HT and F_4TCNQ in the in-plane direction. In addition, a diffuse amorphous scattering centered on $q \approx 1.35$ Å^{-1} appears whose intensity increases with doping time.

Vapor doping at elevated temperature assists diffusion of dopants into the side chains of the polymer. During vapor doping process in our experimental setup, the P3HT film reaches temperatures of ≈80° ± 5 °C, which is well above its glass transition. At this temperature, the film goes through structural changes due to both thermal expansion and infiltration of F_4TCNQ. Figure S4 shows alkyl and π stacking distance change in neat P3HT film during in situ heating GIWAXS measurements. The alkyl stacking distance of neat P3HT film changes from 16.2 Å at room temperature to a spacing of 16.6 Å at 80 °C. In doped films, F_4TCNQ molecules are intercalated between the side chains with a larger alkyl stacking distance of 18.0 Å at room temperature (vide infra). Due to the increased alkyl spacing from thermal expansion during the doping process, F_4TCNQ molecules might be able to diffuse easily to the side chain regions. While there is no report of the temperature dependent diffusion coefficient of F_4TCNQ in P3HT, the diffusion coefficient of PCBM in P3HT is temperature activated and sufficiently high that diffusion is rapid in thin films.[44] Because PCBM has larger volume than F_4TCNQ, this provides a bound with the expectation that diffusion of F_4TCNQ would likely be faster. Furthermore, dopants have longer time to diffuse into the crystallites due to the longer time scale of vapor doping compared to solution or sequential doping.

An important question is whether the doped films are homogeneous, i.e., whether there are regions that are doped differently than others. The distinct shifts in the GIWAXS pattern coincide with emergence of polaron and anion peaks in optical spectra. In the optical spectra, P3HT polaron and F_4TCNQ anion features are seen for films doped for 5 min or longer at concentrations of 4 mol % (Figure 2). The change in the ordered regions of P3HT changes significantly between 0.2 and 4 mol %. The alkyl stacking distance shifts from 16.2 Å below 0.2 mol % to 18.0 Å for greater than 4 mol %. Concomitantly, a single π-stacking peak is observed below 0.2 mol %, and two peaks appearing near the original π stacking peak are observed at 4 mol % (Figure 5). The lack of two alkyl-stacking peaks suggests that the two in-plane features are from the same population; i.e., there is a single structure for the doped phase. The concentration of dopant is sufficiently low at 0.23 mol % that it does not cause noticeable changes in crystal structure or that the F_4TCNQ resides in the amorphous regions of P3HT. This result is consistent with the assessment that the solubility limit of the amorphous region is ≈5%; however, there has been no systematic study of films where the volume fractions of ordered and amorphous domains are quantified to determine if such a value is simply representative of a "typical" film, or if it is representative of a true solubility limit.

The scattering features observed by GIWAXS suggest that the F_4TCNQ molecules are incorporated into the crystallites with likely a small perturbation to the molecular packing at the molecular level. We suspect that dopants are intercalated between alkyl side chains of the polymer based on the structural change as F_4TCNQ is introduced, which results in increased layer spacing and decrease in $\pi-\pi$ spacing. Intercalation of dopants between the polymer backbones has been proposed for solution doped films,[28] but it seems implausible with vapor doping. It is unlikely that the large amount of F_4TNCQ can be inserted between the stacked P3HT backbones through solid-state diffusion. The P3HT backbones would need to separate in the $\pi-\pi$ stacking direction by almost 100% for dopants to intercalate between the backbones. In addition, this would need to propagate through entire P3HT crystals to allow Bragg scattering to be observed. A recent study on aligned P3HT film sequentially doped with F_4TCNQ used a combination of high resolution TEM and polarized UV−vis−IR to propose that dopants are incorporated into the side chains with their long molecular axis perpendicular to the polymer backbone.[6] This model also predicts flattening of alkyl side chain with respect to the thiophene ring, which explains the increase in alkyl stacking distance and decrease in $\pi-\pi$ stacking distance in doped films. The same trend was also shown in the X-ray, electron, and neutron diffraction of P3HT thin films doped with F_4TNCQ molecules in many systems.[1,2,5,21] In contrast, many computational studies of charge transfer interactions examine face-to-face overlap of polythiophenes and F_4TCNQ.[45,19] While charge transfer may not be observed in gas-phase dimers without overlap of wave functions, in solids the Coulomb interaction between the charges is more complex due to long-range interaction of all of the charges and can allow charge transfer over longer distances.[46]

The main difference between the solution and the vapor doping methods is the texture of the crystallites and the change in relative intensities of the in-plane π stacking peaks. Figure S7 shows in-plane scattering intensity of the neat, solution, and vapor-doped films. Solution doped film has a strong in-plane alkyl stacking peak, which comes from face-on crystallites. It clearly suggests that the crystallites in neat and vapor-doped samples have much stronger preference to have edge-on texture compared to those in solution-doped films similar to comparisons of solution and sequentially doped films.[38] The tendency to have a dominant orientation of the crystallites in vapor-doped films should improve transport relative to solution processed films that have a mixture of orientations with differing domain boundaries. In solution doping, the interaction between P3HT and dopant molecules and the formation of aggregates in solution result in solid-state film with more face-on crystalline domains.[13] In sequential and vapor-doped films, the texture of the neat P3HT film is better retained suggesting that the F_4TCNQ does not strongly perturb the morphology of the neat P3HT film. The use of vapor-doping prevents swelling of the film by solvent during sequential casting that could change the morphology.

In addition to the texture, the change in intensity of the in-plane scattering peaks shows a difference for vapor-doped films. The fraction of the integrated intensity of the higher q peak near the original π stacking peak region gradually decreases with increasing dopant concentration for vapor-doped samples while that of the solution doped samples remains relatively constant[13] (Table S4). In vapor doped films, the fraction gradually decreases from 1 in neat and 2 min doped (0.23 mol

DOI: 10.1021/acs.chemmater.7b04849
Chem. Mater. 2018, 30, 998−1010

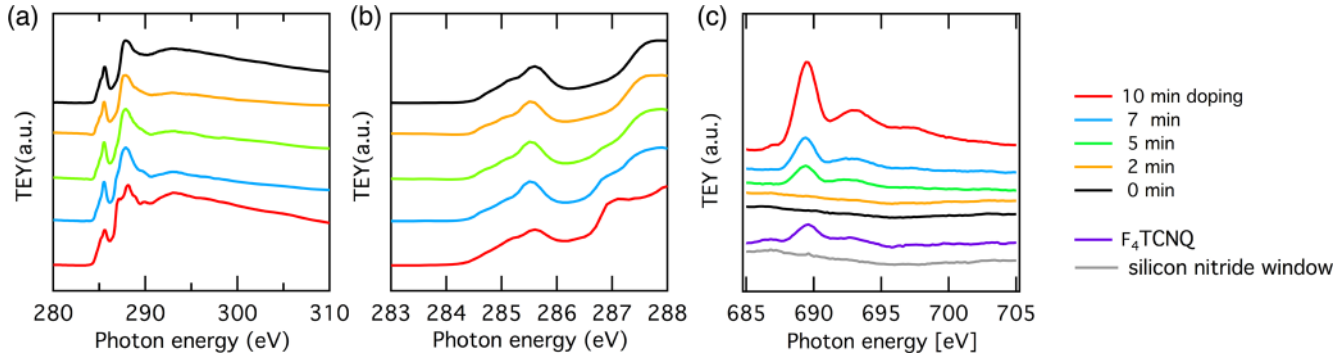

Figure 6. (a) and (b) NEXAFS spectra of P3HT films vapor-doped with F_4TCNQ at the C K-edge. Features at 285.4 and 287 eV arise from doping due to F_4TCNQ anion. (c) NEXAFS spectra at the F K-edge.

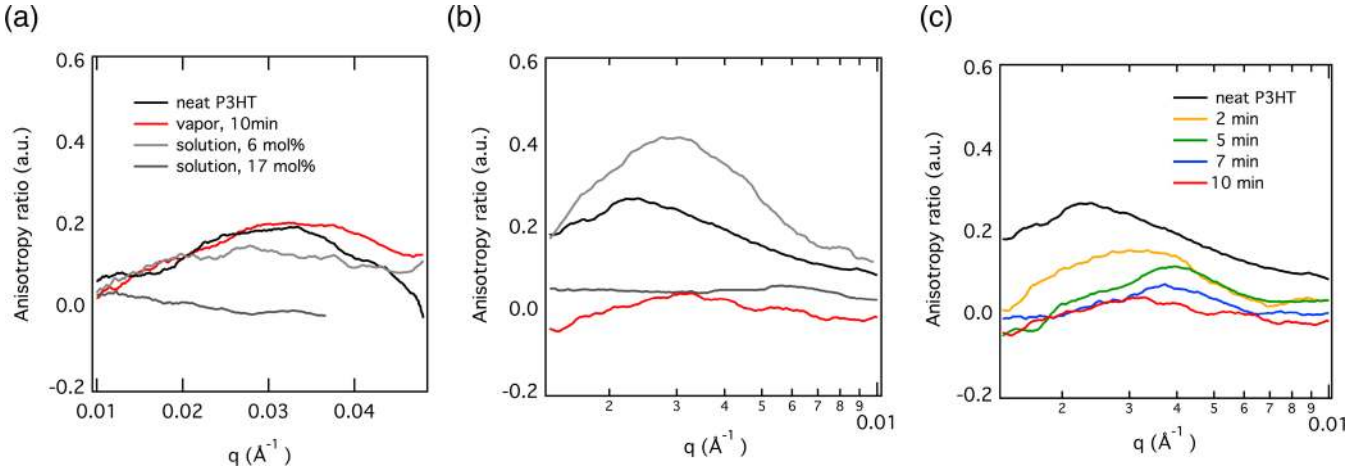

Figure 7. Anisotropy ratio of neat and doped P3HT films at 285.4 eV. Anisotropy ratio is calculated as $(I_{180°} - I_{90°})/(I_{180°} + I_{90°})$. Anisotropy ratios of neat, solution, and vapor-doped films at (a) high q and (b) low q range are shown. (c) Anisotropy ratio of films vapor-doped for various times at high q range.

%) film to 0.64 in 10 min doped (10 mol %). Solution doped samples had one peak up to 1.2 mol %, and the two peaks well separated with constant fraction at doping levels from 3 to 17 mol %.[13,38] If the two peaks are not representative of two phases, then it suggests that there may be a difference in the structure factor of the scattering peak from vapor doping. Detailed modeling that incorporates disorder is required to study this effect, however. In contrast, the PBTTT:F_4TCNQ does not show an obvious difference in local structure compared to films prepared by different solution doping methods.[26,15] Additionally, while the change in d-spacing is gradual for PBTTT:F_4TCNQ,[47] the d-spacing for P3HT:F_4TCNQ is bimodal, occurring around 5 min doping. The ratio of the intensities of the in-plane peak, as well as more preferential edge-on texture, observed in vapor-doped samples could be related to the higher electrical conductivity measured for vapor doped samples than solution doped samples at similar dopant concentrations.

Resonant Soft X-ray Scattering (RSoXS) Reveals Long-Range Connectivity in Doped Films. The local structure of P3HT films doped by F_4TCNQ shows small differences in structure with the largest difference being the texture of the crystalline domains. This observation suggests that the longer-range morphology likely has an important role in determining the electrical conductivity. Atomic force microscopy showed no clear sign of change in morphology at the surface that would affect the charge transport (Figure S8). We therefore used small angle X-ray scattering to determine if there were obvious changes in domain size between the two processing methods.

Morphological features in longer length scales from both crystalline and amorphous regions in the bulk are studied using RSoXS by using energy near the resonant edge of the chemical element. Near edge X-ray absorption fine structure (NEXAFS) spectra provide spectral information on transitions during which electrons are excited from core to higher level unoccupied states. By tuning the incident energy, the scattering contrast is derived from change in scattering length density near the resonant edge of the chemical element.[48] Figure 6 shows NEXAFS spectra of P3HT and doped films near the carbon and fluorine K-edge. The peak near 285.4 eV is characteristic of the 1s to π^* transition from the C═C bond in P3HT. Upon doping, there is a small increase in absorption from F_4TCNQ at 285.4 eV (Figure S10), but no clear shift or change is observed in the P3HT features. Shoulders at 287 and 288.9 eV arise from the F_4TCNQ anion. NEXAFS spectra at the fluorine K-edge show emergence and increase of the F_4TCNQ peak after 5 min of doping.

The RSoXS scattering pattern of P3HT is complex due to the presence of crystalline and amorphous domains. Ordered regions of P3HT are known to form fibrils which may have face-on or edge-on texture of the conjugated backbone relative to the substrate. The face-on and edge-on populations interact differently with the incident polarized X-ray beam due to the difference in orientation of their transition dipole moment

DOI: 10.1021/acs.chemmater.7b04849
Chem. Mater. 2018, 30, 998−1010

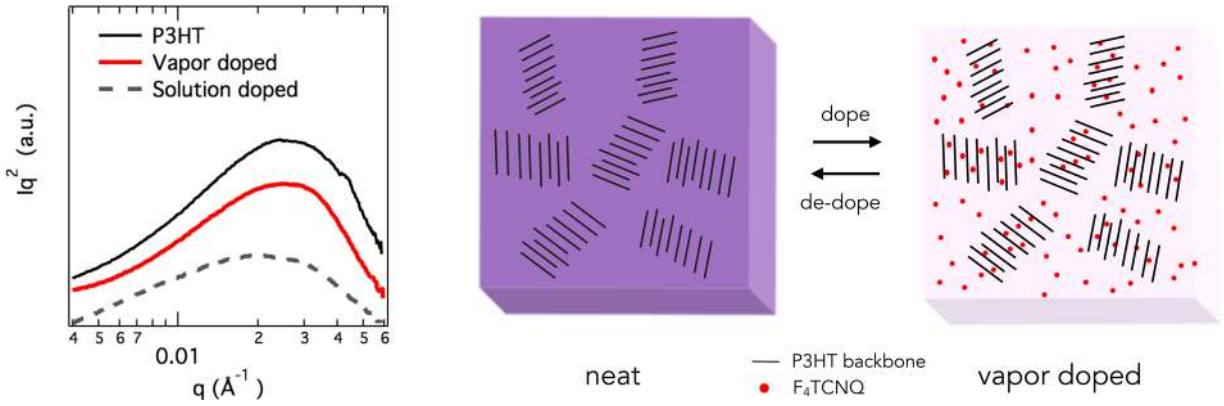

Figure 8. (left) Lorentz corrected, radially integrated RSoXS scattering profiles of doped films at photon energy of 285.4 eV. Black: annealed neat P3HT film. Blue: vapor doped film. Gray: Solution-doped film. (right) Schematic of thin film morphology before and after vapor-doping.

relative to the electric field vector of the X-ray. The orientation of the fibrils would likely depend on processing conditions, as well as molecular weight, and has been previously shown to contribute to anisotropy in the scattering pattern.[49−51]

The polarized RSoXS of neat P3HT film (at $E_{incident}$ = 285.4 eV) shows peaks in the scattering near 0.003 Å^{-1} and 0.03 Å^{-1} with significant anisotropy with their direction perpendicular to each other. We attribute these features to different morphological features of the P3HT films. The peak and associated anisotropy at 0.03 Å^{-1} comes from the form factor of the fibrils (Figure S11). Due to the linearly polarized incident beam, the stiff, orientationally correlated segments of the backbone have orientation with respect to the polarization direction, which results in anisotropy in scattering. The anisotropy near 0.003 Å^{-1} comes from the domain boundary between P3HT fibrils and amorphous regions of the film (Figure S12). In a simplified model where the P3HT fibrils have a rectangular shape, the fibrils can have two different types of interface with the amorphous regions, one in which the polymer backbone is perpendicular to the interface, another one in which the polymer backbone is parallel to the interface. The difference in the amount of these interfaces, which is determined by the form factor of the fibrils, can lead to the scattering anisotropy. This anisotropy is in agreement with a recent study where long fibrils lead to anisotropy in this q range, but shorter stacks with a relatively similar amount of parallel and perpendicular interfaces between crystalline and amorphous regions show lack of anisotropy.[49]

The vapor-doped films have long fibrils of P3HT with dopant molecules having preferential orientation with respect to the polymer backbone in crystalline regions and random orientation at the crystalline/amorphous interface and in amorphous regions. We collected RSoXS patterns for P3HT films as a function of the concentration of F_4TCNQ to determine if the infiltration of the dopant influenced the morphology. Figure 7a shows that the anisotropy parameter near 0.03 Å^{-1} of vapor-doped film is 0.2, which remains unchanged from that of the neat film. As our vapor-doped film likely maintains the initial morphology of the undoped P3HT film, the form factor of the P3HT fibrils in vapor-doped film is expected to be the same as that of the neat film. On the other hand, the anisotropy near 0.003 Å^{-1} decreases and eventually disappears with increase in dopant concentration (Figure 7c), due to the F_4TCNQ dopants at crystalline/amorphous domain interface having random orientation with respect to the P3HT backbone in the fibrils. At high doping levels, the crystalline and amorphous interfaces no longer have two different types of interfaces because of the disorder in the orientation of F_4TCNQ at the interface and its contribution to the contrast making the ordered and amorphous regions similar. The disappearance of anisotropy arises from the change in contrast due to the absorption of F_4TCNQ near the scattering energy. In contrast, a dopant that does not absorb at this energy would exhibit no change in scattering. De-doping the films further proves this model. As we de-dope the film, the F_4TCNQ dopants leave, the film is left with preferentially oriented P3HT at amorphous/crystalline domain interface, and the anisotropy reappears. We do not suspect that the disappearance (reappearance) of anisotropy upon doping (de-doping) is due to a resonant energy shift upon doping (Figure S13). The scattering peak at 0.03 Å^{-1} is strong and only observed at 285.4 eV even after doping. Additionally, the total scattering count from the energy scan around this energy shows that the scattering is still the strongest at 285.4 eV after doping.

Solution-doped films form shorter fibrils with preferentially oriented crystalline−amorphous domain boundaries. Figure 7a shows that the anisotropy parameter is around 0.2 for neat, heavily vapor-doped films and low-solution doped samples while heavily solution doped film shows no anisotropy. The absence of anisotropy in the heavily solution dope film is due to shorter fibrils formed from aggregation in the solution state, resulting in a smaller form factor (square-like rather than rectangular crystals). Formation of shorter stacks in solution-doped P3HT has also been shown in a previous study where aggregate formation in dopant/polymer solution results in shorter stacks in solid state compared to neat P3HT films.[52] In low solution doped (∼6 mol %) film, the anisotropy near 0.003 Å^{-1} is higher than that in neat or vapor-doped, suggesting preferential orientation of the domain boundaries (Figure 7b). At high doping level (17 mol %), this anisotropy disappears even with preferential orientation of dopants at domain boundaries, due to the short fibrils.

With the bond sensitivity and the orientational sensitivity, an orientation correlation length (OCL) can be calculated from RSoXS. In conjugated molecules, 1s to π^* transition dipole moments point in direction perpendicular to the plane of the backbone. The OCL is a length over which conjugated polymer backbones retain their orientational correlation with their neighbors. This length scale is relevant to the charge transport in thin film devices. Because the charge transport in semiconducting polymers is the fastest along the conjugated backbone, the longer the orientational correlation length is, the

DOI: 10.1021/acs.chemmater.7b04849
Chem. Mater. 2018, 30, 998−1010

easier it would be for the charges to travel over a long distance. The OCL has been shown to have a good correlation with conductivity and saturation mobility in organic thin film transistors.[15,53,54]

The RSoXS scattering profiles suggest that the long-range connectivity of the vapor-doped film does not change upon diffusion of F_4TCNQ molecules in solid state. Figure 8 shows Lorentz corrected RSoXS profiles of neat and doped P3HT films at 285.4 eV, and the half of the *d*-spacing corresponding to the peak location is suggested to be the polymer backbone OCL. The OCLs of the neat and vapor-doped films are about 12 nm, which is in a good agreement with the size of the crystalline lamellae plus the amorphous interlamellar zone for regioregular P3HT observed with high resolution TEM.[55] The scattering profile of the solution-doped sample has a broader peak centered slightly to the lower *q*, with OCL of 14 nm.

The similar OCL of solution and vapor doped samples potentially explains the smaller change in maximum conductivities measured from films prepared by these two methods. As noted previously, the maximum conductivity measured in vapor- doped P3HT:F_4TCNQ film was about 20 times higher than that of solution doped films compared to about 100 times higher in PBTTT:F_4TCNQ. In PBTTT:F_4TCNQ, the reported OCLs for solution and vapor doped samples are 80 and 215 nm with conductivities of 2 S/cm and 220 S/cm, respectively, correlating well with the over hundredfold increase in electrical performance. Figure S14 shows previously reported conductivity of heavily vapor-doped PBTTT samples and their OCLs.[15] Interestingly, as we extrapolate the trend line for the electrical conductivity vs the OCL from the heavily vapor-doped PBTTT data, the conductivity of heavily vapor-doped P3HT from this study sits directly on the extrapolated line. Furthermore, aligned P3HT films have shown higher mobility and conductivity along the backbone alignment direction, supporting the correlation between the orientation correlation and carrier mobility.[6,23,28,56] Rubbing aligned P3HT film that was sequentially doped with F_4TCNQ had conductivity of 22 S/cm in the aligned direction, about 7 times higher than the conductivity of 3 S/cm in the unaligned samples. Stretch aligned P3HT film doped by vacuum evaporation of F_4TCNQ had 19 times higher conductivity in the aligned film parallel to the stretch direction compared to nonstretched film. These results further support the relationship between the charge transport and the long-range connectivity of the crystalline domains in semiconducting polymer thin films. Overall, while OCL is potentially a critical factor that governs mobility of semicrystalline polymers, other factors such as the texture of ordered domains and the local structure of π stacked chains also affect the mobility.

Effect of Vapor-Doping on Thermopower. Thermoelectric materials are benchmarked by a figure of merit that is determined by a combination of the Seebeck coefficient, *S*, the electrical conductivity, σ, and the thermal conductivity, κ, known as $ZT = S^2\sigma/\kappa$. The power factor (PF) of a thermoelectric is equal to the product of the electrical conductivity and the square of the Seebeck coefficient.[32] The thermopower (Seebeck coefficient) of a semiconductor is related to the Fermi level within the electronic density of states, i.e., the carrier concentration and, for polaronic materials, also has vibronic contributions.[58,59] The thermoelectric performance of a semiconducting polymer's thermopower is currently difficult to predict due to the interplay of doping and morphology.[57] Because the electrical conductivity can change dramatically with comparable levels of doping due to processing, it is important to examine the impact on the thermopower.

Films of P3HT doped by F_4TCNQ from vapor have a higher thermopower than those doped in solvent. We have found an empirical correlation between the thermopower and electrical conductivity across a wide range of materials that scales as $S \propto \sigma^{-1/4}$;[15,25] others have suggested an exponent of $-1/3$ depending on the data set chosen for the fit.[60] This trend is purely empirical and provides an estimate of an approximate value of the thermopower for a given electrical conductivity. In our vapor-doped films, Seebeck coefficients of 85 ± 10 μV/K were measured for samples with conductivity around $\sim 10^1$ S/cm. Figure 9a shows the Seebeck coefficient of P3HT films as a function of conductivity from this study and from films solution doped with F_4TCNQ reported in previous studies.[25,61] For a P3HT solution doped with 17 mol % F_4TCNQ, the Seebeck coefficient was measured to be 76 μV/K with a conductivity of 2 S/cm. Previously, Seebeck coefficients of ~100 μV/K with

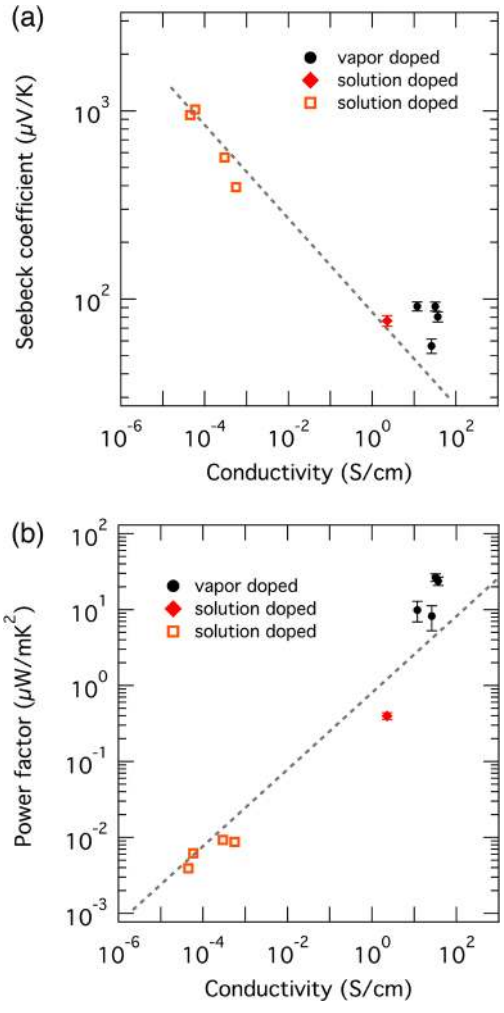

Figure 9. (a) Seebeck coefficient and (b) power factor of P3HT thin films as a function of conductivity. Black: vapor -doped with F_4TCNQ, red/orange: solution doped with F_4TCNQ. Vapor-doped samples were at various doping concentrations of 5 to 10 mol %. Red diamond: concentration of solution doped film from this study was 17 mol % F_4TCNQ. Orange square: solution doped films from literature were 0.6 to 3 mol % F_4TCNQ. Dotted gray lines are previously reported empirical trends [$\alpha \propto \sigma^{-1/4}$, PF $\propto \sigma^{1/2}$, ref 25].

DOI: 10.1021/acs.chemmater.7b04849
Chem. Mater. 2018, 30, 998−1010

conductivities ranging 10^{-5} to 10^{-3} S/cm were reported for solution-doped P3HT films with 0.6 to 3 mol % F_4TCNQ.[25] The empirical prediction suggests that the thermopower is enhanced for the vapor-doped samples leading to an improvement in the PF (Figure 9b).

The empirical trend uses the electrical conductivity as a surrogate for the carrier concentration, but we can also compare our results to results in literature for doped P3HT at comparable carrier concentrations. While different counterion species could potentially have impact on the Seebeck coefficient due to interactions between the carrier and the ion, it is currently not possible to disaggregate such effects from the carrier concentration and morphology. For our most heavily doped samples at an estimated carrier concentration of 5×10^{20} cm^{-3}, we find that $S = 85 \pm 10$ μV/K. For P3HT doped in solution with F_4TCNQ we find a lower value, $S = 76 \pm 3$ μV/K, at 6×10^{20} cm^{-3}. We can compare these results to P3HT doped by immersion in a solution of Fe(III) triflimide ($TFSI^-$) at a slightly higher carrier concentration of 1.2×10^{21} cm^{-3} where $S = 31$ μV/K.[62] The electrical conductivity, mobility, and doping level of the immersion doped P3HT were higher at 180 S/cm, 1 cm^2 V^{-1} s^{-1}, and 0.3 charge/monomer of P3HT than those of our F_4TCNQ vapor-doped sample at 48 S/cm, 0.6 cm^2 V^{-1} s^{-1}, and 0.1 charge/monomer of P3HT. Despite the difference in electrical conductivity the PF of the vapor-doped sample is 27 $\mu W/mK^2$ and agrees within error to that of P3HT immersion doped with $TFSI^-$ at 22 $\mu W/mK^2$.[25] This observation suggests that it should be possible to further optimize the trade-off between increasing electrical conductivity and decreasing Seebeck coefficient by controlling processing.

Using the measured morphology of the doped films, we can begin to separate the factors controlling the connection between the electrical conductivity and thermopower. For solution and vapor-doped P3HT, the thermopower and OCL were 76 ± 3 μV/K and 14 nm and 85 ± 10 μV/K and 12 nm, respectively. While the carrier mobilities in these films differ by about 30 times, their OCLs and Seebeck coefficients are comparable. This comparison suggests that, in P3HT, the impediment to charge transport in cast films does not greatly impact the Seebeck coefficient. It has been suggested that local disorder controls the electronic density of states of P3HT with the connectivity by tie-chains aiding transport.[63] Because the slope of the density of states near the Fermi level (given by Seebeck coefficient) is comparable in the two doped films at comparable carrier concentration, it would imply that the density of states is very similar and that the increase in electrical conductivity is impacted by the connectivity of the domains. In contrast to the behavior of P3HT, the thermopower appears to have a stronger dependence on morphology for solution and vapor-doped PBTTT:F_4TCNQ. At a comparable carrier concentration, the thermopower changed from 60 μV/K to 30 μV/K with a change in OCL from 40 to 350 nm with greater than 100 times change in electrical conductivity.[15] In the case of PEDOT:PSS, where the size of the PEDOT domains is similar to that of P3HT, significantly higher conductivity is observed despite it having a low molecular weight with likely few tie chains.[64] It is currently not known if the smaller side chains on PEDOT could enable improved hopping between domains with varying orientation that is not possible with the longer alkyl chains on other polymers such as P3HT. More detailed transport and thermopower measurements are necessary to make quantitative conclusions about the changes in the density of states and transport as a function of processing between these materials.

CONCLUSIONS

Doping from the vapor phase is an effective way of studying molecular doping in semiconducting polymers as it minimizes the morphology dependent changes in electrical conductivity. With P3HT and the molecular dopant F_4TCNQ, we have found that conductivity can be tuned with vapor phase doping. F_4TCNQ is incorporated into the side chains of P3HT maintaining the crystalline order in cast films. While different doping methods have little effect on the long-range connectivity in doped P3HT films, the crystallite texture and fibril length of P3HT thin film change dramatically with processing method. In order to achieve higher mobility and conductivity in doped P3HT films, it would be necessary to use processing methods to further increase the long-range connectivity of the polymer while controlling the texture and fibril length for efficient charge transport in the solid state.

The ability to maintain the morphology of P3HT films during vapor-doping also allowed us to study the effect of morphology on thermoelectric properties. Using either solution or vapor doping, films of P3HT:F_4TCNQ with comparable OCL and carrier concentration had similar Seebeck coefficients. The higher electrical conductivity of vapor-doped films led to higher thermoelectric power factors than for solution-doped films. Furthermore, this methodology will allow for detailed study of temperature dependent conductivity and Seebeck measurements to provide further insight into transport mechanism in these films. In emerging designs for thin film organic thermoelectric generators, such as radial,[65] coiled, or corrugated modules,[66,67] films on the order of 1 to 10 μm may be required. Further investigation into the changes in performance upon processing films with such thicknesses will be required to determine if the improvements here can be realized in thicker films.[27]

EXPERIMENTAL SECTION

Materials. P3HT was purchased from Merck (SP001, M_n = 50 000; M_w = 79 000; RR = 95%) and used as received without further purification. The small molecule F_4TCNQ was purchased from TCI America. The anhydrous solvents *ortho*-dichlorobenzene and chlorobenzene were purchased from Sigma-Aldrich.

Thin Film Preparation. Thin film samples for GIWAXS experiments were prepared on Si/SiO_2 wafers. Films for electrical characterization was prepared on a 0.5 mm thick Z-cut quartz wafer from University wafer. Substrates were sequentially sonicated for 15 min in soapy water, DI water, acetone, and isopropanol. Films for NEXAFS and RSoXS were prepared on silicon nitride windows with a 200 μm thick Si_3N_4 layer. For vapor doping, neat P3HT was dissolved in 1:1 ODCB:CB solvent mixture (5 mg/mL). Thin films were spun cast using a two-step spin condition of 1000 rpm for 45 s followed by 3000 rpm for 30 s. Thin films were soft baked at 150 °C for 1 min to remove excess solvent. Then the films were annealed at 150 °C for 10 min under N_2 environment. Thicknesses of films were 20−25 nm. F_4TCNQ powder was heated to 210 °C in a custom closed-vessel doping chamber. The temperature of the film was 80 °C during vapor doping, and the amount of dopant was controlled by the time during which film was exposed to the vaporized dopant. Vaporized F_4TCNQ was deposited to P3HT film for 0 to 15 min. For solution doping, 5 mg/mL F_4TCNQ in 1:1 ODCB:CB was added to the neat P3HT solution. Thin films were spun cast directly from the solution mixture.UV−vis absorption spectra were collected with a Shimadzu UV3600 spectrometer.

DOI: 10.1021/acs.chemmater.7b04849
Chem. Mater. 2018, 30, 998−1010

Grazing Incidence X-ray Diffraction. Grazing incidence X-ray scattering experiments were conducted at the Advanced Light Source at beamline 7.3.3. The energy of the incident beam was at 10 keV, and a Pilatus 2 M area detector was used. The X-ray scattering data were taken at incidence angles of 0.14° with 1−5 s exposure times. The samples were kept under helium environment during X-ray exposure to minimize air scattering and sample degradation.[68,69] The collected data were processed using Nika, a 2D data reduction macro on Igor Pro using established procedures. Diffraction pattern from silver behenate was used to calibrate the beam center and the sample-to-detector distance. 1D profiles were created by plotting intensities along the line cuts near $q_y = 0$ and $q_z = 0$, with a correction for the grazing incidence geometry.

Near Edge X-ray Absorption Fine Structure Spectroscopy (NEXAFS). NEXAFS spectroscopy was performed at beamline 11.0.1.2 at the Advanced Light Source. The beamline has an incident photon energy flux of about 1×10^{13} photons/s at 800 eV. The beam spot size was 0.1 mm × 0.1 mm at 90° incidence angle. C, N, and F K-edge NEXAFS spectra were collected from incident photon energies from 270 to 710 eV. The X-ray beam was linearly polarized in the horizontal or vertical direction. The sample stage was computer-controlled to set the angle of the substrate surface with respect to the incoming X-ray. The total electron yield (TEY) data was collected at an incident angle of 45° to increase the footprint of the beam spot on the sample and improve signal. The absorption spectra were normalized by incident beam intensity as well as the signal intensity through a blank silicon nitride window.

Resonant Soft X-ray Scattering (RSoXS). RSoXS was performed at beamline 11.0.1.2 at the Advanced Light Source. Sample was placed in a high vacuum chamber, and transmission geometry was used. Data were collected with in-vacuum CCD detector, and dark image background noise was subtracted. Vertically and horizontally polarized photons at an energy of 285.4 eV were used to obtain anisotropic scattering patterns. Scattering patterns were radially integrated as a function of the scattering vector and plotted with a Lorentz correction (Iq^2 vs q).

Electrical Characterization. Gold electrical contacts (60 nm thick) were deposited onto the neat P3HT films before vapor doping and the solution doped films via controlled thermal evaporation through a shadow mask. Contacts for electrical conductivity and thermopower measurements were prepared on the same film. Electrical conductivity was measured in the in-plane direction with four-point probe geometry. Thermopower was measured with two 1 mm^2 gold pads, a set of 0.2 mm × 1 mm contacts that are 3 to 5 mm apart, using the previously reported differential method.[25] All electrical measurements were made under N_2 environment inside a glovebox. The Seebeck coefficient had error of ≈10% from sample to sample variation and contributions from the electrical leads, the accuracy of temperature difference, and geometrical error.[70]

Atomic Force Microscopy (AFM). Film thicknesses, topology, and phase images were obtained on Asylum MFP-3D using tapping mode.

■ ASSOCIATED CONTENT

Supporting Information

The Supporting Information is available free of charge on the ACS Publications website at DOI: 10.1021/acs.chemmater.7b04849.

Additional details regarding UV−vis, GIWAXS, RSoXS, AFM micrographs, and electrical properties (PDF)

■ AUTHOR INFORMATION

Corresponding Author

*(M.L.C.) E-mail: mchabinyc@engineering.ucsb.edu.

ORCID

Michael L. Chabinyc: 0000-0003-4641-3508

Author Contributions

The manuscript was written through contributions of all authors. All authors have given approval to the final version of the manuscript.

Notes

The authors declare no competing financial interest.

■ ACKNOWLEDGMENTS

This work was supported by NSF DMR 1410438. E.L. received support from a National Science Foundation Graduate Research Fellowships (DGE-1144085). Portions of the research were carried out at the Advanced Light Source, supported by the Director, Office of Science, Office of Basic Energy Sciences, of the U.S. Department of Energy under Contract No. DE-AC02-05CH11231. The research reported here made use of shared facilities of the UCSB MRSEC (NSF DMR 1720256), a member of the Materials Research Facilities Network (www.mrfn.org)

■ REFERENCES

(1) Arkhipov, V. I.; Emelianova, E. V.; Tak, Y. H.; Bässler, H. Charge Injection into Light-Emitting Diodes: Theory and Experiment. *J. Appl. Phys.* **1998**, *84* (2), 848−856.

(2) Hoppe, H.; Sariciftci, N. S. Organic Solar Cells: An Overview. *J. Mater. Res.* **2004**, *19* (7), 1924−1945.

(3) Campbell, I. H.; Rubin, S.; Zawodzinski, T. A.; Kress, J. D.; Martin, R. L.; Smith, D. L.; Barashkov, N. N.; Ferraris, J. P. Controlling Schottky Energy Barriers in Organic Electronic Devices Using Self-Assembled Monolayers. *Phys. Rev. B: Condens. Matter Mater. Phys.* **1996**, *54* (20), R14321−R14324.

(4) Mihailetchi, V. D.; Blom, P. W. M.; Hummelen, J. C.; Rispens, M. T. Cathode Dependence of the Open-Circuit Voltage of Polymer:-fullerene Bulk Heterojunction Solar Cells. *J. Appl. Phys.* **2003**, *94* (10), 6849−6854.

(5) Kim, G.-H.; Shao, L.; Zhang, K.; Pipe, K. P. Engineered Doping of Organic Semiconductors for Enhanced Thermoelectric Efficiency. *Nat. Mater.* **2013**, *12* (8), 719−723.

(6) Zhang, Q.; Sun, Y.; Xu, W.; Zhu, D. Organic Thermoelectric Materials: Emerging Green Energy Materials Converting Heat to Electricity Directly and Efficiently. *Adv. Mater.* **2014**, *26* (40), 6829−6851.

(7) Russ, B.; Glaudell, A.; Urban, J. J.; Chabinyc, M. L.; Segalman, R. A. Organic Thermoelectric Materials for Energy Harvesting and Temperature Control. *Nat. Rev. Mater.* **2016**, *1* (10), 16050.

(8) Jacobs, I. E.; Moulé, A. J. Controlling Molecular Doping in Organic Semiconductors. *Adv. Mater.* **2017**, *29* (42), 1703063.

(9) Scholes, D. T.; Hawks, S. A.; Yee, P. Y.; Wu, H.; Lindemuth, J. R.; Tolbert, S. H.; Schwartz, B. J. Overcoming Film Quality Issues for Conjugated Polymers Doped with F_4TCNQ by Solution Sequential Processing: Hall Effect, Structural, and Optical Measurements. *J. Phys. Chem. Lett.* **2015**, *6* (23), 4786−4793.

(10) Zheng, W.; Min, Y.; MacDiarmid, A. G.; Angelopoulos, M.; Liao, Y.-H.; Epstein, A. J. Aggregation and Molecular Conformation of Doped Polyaniline in Chloroform Solution. *Synth. Met.* **1997**, *84* (1), 109−110.

(11) McFarland, F. M.; Bonnette, L. R.; Acres, E. A.; Guo, S. The Impact of Aggregation on the P-Doping Kinetics of poly(3-Hexylthiophene). *J. Mater. Chem. C* **2017**, *5* (23), 5764−5771.

(12) Pingel, P.; Neher, D. Comprehensive Picture of *p*-Type Doping of P3HT with the Molecular Acceptor F_4TCNQ. *Phys. Rev. B: Condens. Matter Mater. Phys.* **2013**, *87* (11), 115209.

(13) Duong, D. T.; Wang, C.; Antono, E.; Toney, M. F.; Salleo, A. The Chemical and Structural Origin of Efficient p-Type Doping in P3HT. *Org. Electron.* **2013**, *14* (5), 1330−1336.

(14) Jacobs, I. E.; Moulé, A. J. Controlling Molecular Doping in Organic Semiconductors. *Adv. Mater.* **2017**, *29*, 1703063.

DOI: 10.1021/acs.chemmater.7b04849
Chem. Mater. 2018, 30, 998−1010

(15) Patel, S. N.; Glaudell, A. M.; Peterson, K. A.; Thomas, E. M.; O'Hara, K. A.; Lim, E.; Chabinyc, M. L. Morphology Controls the Thermoelectric Power Factor of a Doped Semiconducting Polymer. *Sci. Adv.* **2017**, *3* (6), e1700434.
(16) Gao, J.; Roehling, J. D.; Li, Y.; Guo, H.; Moulé, A. J.; Grey, J. K. The Effect of 2,3,5,6-Tetrafluoro-7,7,8,8-Tetracyanoquinodimethane Charge Transfer Dopants on the Conformation and Aggregation of poly(3-Hexylthiophene). *J. Mater. Chem. C* **2013**, *1* (36), 5638−5646.
(17) Yim, K.-H.; Whiting, G. L.; Murphy, C. E.; Halls, J. J. M.; Burroughes, J. H.; Friend, R. H.; Kim, J.-S. Controlling Electrical Properties of Conjugated Polymers via a Solution-Based P-Type Doping. *Adv. Mater.* **2008**, *20* (17), 3319−3324.
(18) Wang, C.; Duong, D. T.; Vandewal, K.; Rivnay, J.; Salleo, A. Optical Measurement of Doping Efficiency in poly(3-Hexylthiophene) Solutions and Thin Films. *Phys. Rev. B: Condens. Matter Mater. Phys.* **2015**, *91* (8), 085205.
(19) Gao, J.; Roehling, J. D.; Li, Y.; Guo, H.; Moulé, A. J.; Grey, J. K. The Effect of 2,3,5,6-Tetrafluoro-7,7,8,8-Tetracyanoquinodimethane Charge Transfer Dopants on the Conformation and Aggregation of poly(3-Hexylthiophene). *J. Mater. Chem. C* **2013**, *1* (36), 5638−5646.
(20) Müller, L.; Nanova, D.; Glaser, T.; Beck, S.; Pucci, A.; Kast, A. K.; Schröder, R. R.; Mankel, E.; Pingel, P.; Neher, D.; Kowalsky, W.; Lovrincic, R. Charge-Transfer−Solvent Interaction Predefines Doping Efficiency in P-Doped P3HT Films. *Chem. Mater.* **2016**, *28* (12), 4432−4439.
(21) Scholes, D. T.; Yee, P. Y.; Lindemuth, J. R.; Kang, H.; Onorato, J.; Ghosh, R.; Luscombe, C. K.; Spano, F. C.; Tolbert, S. H.; Schwartz, B. J. The Effects of Crystallinity on Charge Transport and the Structure of Sequentially Processed F4TCNQ-Doped Conjugated Polymer Films. *Adv. Funct. Mater.* **2017**, *27*, 1702654.
(22) Jacobs, I. E.; Aasen, E. W.; Oliveira, J. L.; Fonseca, T. N.; Roehling, J. D.; Li, J.; Zhang, G.; Augustine, M. P.; Mascal, M.; Moulé, A. J. Comparison of Solution-Mixed and Sequentially Processed P3HT: F4TCNQ Films: Effect of Doping-Induced Aggregation on Film Morphology. *J. Mater. Chem. C* **2016**, *4* (16), 3454−3466.
(23) Yasuda, T. Anisotropic Carrier Transport Properties of Stretch-Oriented π-Conjugated Polymers in Organic Field-Effect Transistors. *Phys. Status Solidi C* **2011**, *8* (2), 604−606.
(24) Patel, S. N.; Glaudell, A. M.; Kiefer, D.; Chabinyc, M. L. Increasing the Thermoelectric Power Factor of a Semiconducting Polymer by Doping from the Vapor Phase. *ACS Macro Lett.* **2016**, *5* (3), 268−272.
(25) Glaudell, A. M.; Cochran, J. E.; Patel, S. N.; Chabinyc, M. L. Impact of the Doping Method on Conductivity and Thermopower in Semiconducting Polythiophenes. *Adv. Energy Mater.* **2015**, *5* (4), 1401072.
(26) Kang, K.; Watanabe, S.; Broch, K.; Sepe, A.; Brown, A.; Nasrallah, I.; Nikolka, M.; Fei, Z.; Heeney, M.; Matsumoto, D.; Marumoto, K.; Tanaka, H.; Kuroda, S.; Sirringhaus, H. 2D Coherent Charge Transport in Highly Ordered Conducting Polymers Doped by Solid State Diffusion. *Nat. Mater.* **2016**, *15* (8), 896−902.
(27) Hynynen, J.; Kiefer, D.; Yu, L.; Kroon, R.; Munir, R.; Amassian, A.; Kemerink, M.; Müller, C. Enhanced Electrical Conductivity of Molecularly P-Doped Poly(3-Hexylthiophene) through Understanding the Correlation with Solid-State Order. *Macromolecules* **2017**, *50*, 8140.
(28) Méndez, H.; Heimel, G.; Winkler, S.; Frisch, J.; Opitz, A.; Sauer, K.; Wegner, B.; Oehzelt, M.; Röthel, C.; Duhm, S.; Többens, D.; Koch, N.; Salzmann, I. Charge-Transfer Crystallites as Molecular Electrical Dopants. *Nat. Commun.* **2015**, *6*, 8560.
(29) Hamidi-Sakr, A.; Biniek, L.; Bantignies, J.-L.; Maurin, D.; Herrmann, L.; Leclerc, N.; Lévêque, P.; Vijayakumar, V.; Zimmermann, N.; Brinkmann, M. A Versatile Method to Fabricate Highly In-Plane Aligned Conducting Polymer Films with Anisotropic Charge Transport and Thermoelectric Properties: The Key Role of Alkyl Side Chain Layers on the Doping Mechanism. *Adv. Funct. Mater.* **2017**, *27*, 1700173.
(30) McMahon, D. P.; Cheung, D. L.; Goris, L.; Dacuña, J.; Salleo, A.; Troisi, A. Relation between Microstructure and Charge Transport in Polymers of Different Regioregularity. *J. Phys. Chem. C* **2011**, *115* (39), 19386−19393.
(31) Rossi, G.; Chance, R. R.; Silbey, R. Conformational Disorder in Conjugated Polymers. *J. Chem. Phys.* **1989**, *90* (12), 7594−7601.
(32) Ghosh, R.; Pochas, C. M.; Spano, F. C. Polaron Delocalization in Conjugated Polymer Films. *J. Phys. Chem. C* **2016**, *120* (21), 11394−11406.
(33) Zade, S. S.; Zamoshchik, N.; Bendikov, M. From Short Conjugated Oligomers to Conjugated Polymers. Lessons from Studies on Long Conjugated Oligomers. *Acc. Chem. Res.* **2011**, *44* (1), 14−24.
(34) Pochas, C. M.; Spano, F. C. New Insights on the Nature of Two-Dimensional Polarons in Semiconducting Polymers: Infrared Absorption in poly(3-Hexylthiophene). *J. Chem. Phys.* **2014**, *140* (24), 244902.
(35) Takeda, N.; Miller, J. R. Poly(3-Decylthiophene) Radical Anions and Cations in Solution: Single and Multiple Polarons and Their Delocalization Lengths in Conjugated Polymers. *J. Phys. Chem. B* **2012**, *116* (50), 14715−14723.
(36) Bredas, J. L.; Street, G. B. Polarons, Bipolarons, and Solitons in Conducting Polymers. *Acc. Chem. Res.* **1985**, *18* (10), 309−315.
(37) Colaneri, N.; Nowak, M.; Spiegel, D.; Hotta, S.; Heeger, A. J. Bipolarons in poly(3-Methylthiophene): Spectroscopic, Magnetic, and Electrochemical Measurements. *Phys. Rev. B: Condens. Matter Mater. Phys.* **1987**, *36* (15), 7964−7968.
(38) Scholes, D. T.; Hawks, S. A.; Yee, P. Y.; Wu, H.; Lindemuth, J. R.; Tolbert, S. H.; Schwartz, B. J. Overcoming Film Quality Issues for Conjugated Polymers Doped with F_4TCNQ by Solution Sequential Processing: Hall Effect, Structural, and Optical Measurements. *J. Phys. Chem. Lett.* **2015**, *6* (23), 4786−4793.
(39) Wang, S.; Ha, M.; Manno, M.; Frisbie, C. D.; Leighton, C. Hopping Transport and the Hall Effect near the Insulator−metal Transition in Electrochemically Gated poly(3-Hexylthiophene) Transistors. *Nat. Commun.* **2012**, *3*, 1210.
(40) Arkhipov, V. I.; Emelianova, E. V.; Heremans, P.; Bässler, H. Analytic Model of Carrier Mobility in Doped Disordered Organic Semiconductors. *Phys. Rev. B: Condens. Matter Mater. Phys.* **2005**, *72* (23), 235202.
(41) Arkhipov, V. I.; Heremans, P.; Emelianova, E. V.; Adriaenssens, G. J.; Bässler, H. Charge Carrier Mobility in Doped Semiconducting Polymers. *Appl. Phys. Lett.* **2003**, *82* (19), 3245−3247.
(42) Duong, D. T.; Phan, H.; Hanifi, D.; Jo, P. S.; Nguyen, T.-Q.; Salleo, A. Direct Observation of Doping Sites in Temperature-Controlled, P-Doped P3HT Thin Films by Conducting Atomic Force Microscopy. *Adv. Mater.* **2014**, *26* (35), 6069−6073.
(43) Müller, L.; Nanova, D.; Glaser, T.; Beck, S.; Pucci, A.; Kast, A. K.; Schröder, R. R.; Mankel, E.; Pingel, P.; Neher, D.; Kowalsky, W.; Lovrincic, R. Charge-Transfer−Solvent Interaction Predefines Doping Efficiency in P-Doped P3HT Films. *Chem. Mater.* **2016**, *28* (12), 4432−4439.
(44) Treat, N. D.; Brady, M. A.; Smith, G.; Toney, M. F.; Kramer, E. J.; Hawker, C. J.; Chabinyc, M. L. Interdiffusion of PCBM and P3HT Reveals Miscibility in a Photovoltaically Active Blend. *Adv. Energy Mater.* **2011**, *1* (1), 82−89.
(45) Harrelson, T. F.; Cheng, Y. Q.; Li, J.; Jacobs, I. E.; Ramirez-Cuesta, A. J.; Faller, R.; Moulé, A. J. Identifying Atomic Scale Structure in Undoped/Doped Semicrystalline P3HT Using Inelastic Neutron Scattering. *Macromolecules* **2017**, *50* (6), 2424−2435.
(46) Liu, X. J.; Wang, X. Y.; Zhang, Y. L.; Wang, S.; An, Z. Long-Range Coulomb Interaction Effects on Polarons in Conjugated Polymers. *Org. Electron.* **2015**, *25* (Supplement C), 261−265.
(47) Cochran, J. E.; Junk, M. J. N.; Glaudell, A. M.; Miller, P. L.; Cowart, J. S.; Toney, M. F.; Hawker, C. J.; Chmelka, B. F.; Chabinyc, M. L. Molecular Interactions and Ordering in Electrically Doped Polymers: Blends of PBTTT and F4TCNQ. *Macromolecules* **2014**, *47* (19), 6836−6846.
(48) Wang, C.; Lee, D. H.; Hexemer, A.; Kim, M. I.; Zhao, W.; Hasegawa, H.; Ade, H.; Russell, T. P. Defining the Nanostructured Morphology of Triblock Copolymers Using Resonant Soft X-Ray Scattering. *Nano Lett.* **2011**, *11* (9), 3906−3911.

DOI: 10.1021/acs.chemmater.7b04849
Chem. Mater. 2018, 30, 998−1010

(49) Vakhshouri, K.; Smith, B. H.; Chan, E. P.; Wang, C.; Salleo, A.; Wang, C.; Hexemer, A.; Gomez, E. D. Signatures of Intracrystallite and Intercrystallite Limitations of Charge Transport in Polythiophenes. *Macromolecules* **2016**, *49* (19), 7359−7369.
(50) Kleinhenz, N.; Persson, N.; Xue, Z.; Chu, P. H.; Wang, G.; Yuan, Z.; McBride, M. A.; Choi, D.; Grover, M. A.; Reichmanis, E. Ordering of Poly(3-Hexylthiophene) in Solutions and Films: Effects of Fiber Length and Grain Boundaries on Anisotropy and Mobility. *Chem. Mater.* **2016**, *28* (11), 3905−3913.
(51) Salleo, A. Charge Transport in Polymeric Transistors. *Mater. Today* **2007**, *10* (3), 38−45.
(52) McFarland, F. M.; Ellis, C. M.; Guo, S. The Aggregation of Poly(3-Hexylthiophene) into Nanowires: With and without Chemical Doping. *J. Phys. Chem. C* **2017**, *121* (8), 4740−4746.
(53) Collins, B. A.; Cochran, J. E.; Yan, H.; Gann, E.; Hub, C.; Fink, R.; Wang, C.; Schuettfort, T.; McNeill, C. R.; Chabinyc, M. L.; Ade, H. Polarized X-Ray Scattering Reveals Non-Crystalline Orientational Ordering in Organic Films. *Nat. Mater.* **2012**, *11* (6), 536−543.
(54) Nahid, M. M.; Matsidik, R.; Welford, A.; Gann, E.; Thomsen, L.; Sommer, M.; McNeill, C. R. Unconventional Molecular Weight Dependence of Charge Transport in the High Mobility N-Type Semiconducting Polymer P(NDI2OD-T2). *Adv. Funct. Mater.* **2017**, *27* (9), 1604744.
(55) Brinkmann, M.; Rannou, P. Molecular Weight Dependence of Chain Packing and Semicrystalline Structure in Oriented Films of Regioregular Poly(3-Hexylthiophene) Revealed by High-Resolution Transmission Electron Microscopy. *Macromolecules* **2009**, *42* (4), 1125−1130.
(56) Qu, S.; Yao, Q.; Wang, L.; Chen, Z.; Xu, K.; Zeng, H.; Shi, W.; Zhang, T.; Uher, C.; Chen, L. Highly Anisotropic P3HT Films with Enhanced Thermoelectric Performance via Organic Small Molecule Epitaxy. *NPG Asia Mater.* **2016**, *8* (7), e292.
(57) Kroon, R.; Mengistie, D. A.; Kiefer, D.; Hynynen, J.; Ryan, J. D.; Yu, L.; Müller, C. Thermoelectric Plastics: From Design to Synthesis, Processing and Structure−property Relationships. *Chem. Soc. Rev.* **2016**, *45* (22), 6147−6164.
(58) Xuan, Y.; Liu, X.; Desbief, S.; Leclère, P.; Fahlman, M.; Lazzaroni, R.; Berggren, M.; Cornil, J.; Emin, D.; Crispin, X. Thermoelectric Properties of Conducting Polymers: The Case of poly(3-Hexylthiophene). *Phys. Rev. B: Condens. Matter Mater. Phys.* **2010**, *82* (11), 115454.
(59) Venkateshvaran, D.; Nikolka, M.; Sadhanala, A.; Lemaur, V.; Zelazny, M.; Kepa, M.; Hurhangee, M.; Kronemeijer, A. J.; Pecunia, V.; Nasrallah, I.; Romanov, I.; Broch, K.; McCulloch, I.; Emin, D.; Olivier, Y.; Cornil, J.; Beljonne, D.; Sirringhaus, H. Approaching Disorder-Free Transport in High-Mobility Conjugated Polymers. *Nature* **2014**, *515* (7527), 384.
(60) Kang, S. D.; Snyder, G. J. Charge-Transport Model for Conducting Polymers. *Nat. Mater.* **2017**, *16* (2), 252−257.
(61) Patel, S. N.; Glaudell, A. M.; Kiefer, D.; Chabinyc, M. L. Increasing the Thermoelectric Power Factor of a Semiconducting Polymer by Doping from the Vapor Phase. *ACS Macro Lett.* **2016**, *5* (3), 268−272.
(62) Zhang, Q.; Sun, Y.; Xu, W.; Zhu, D. Thermoelectric Energy from Flexible P3HT Films Doped with a Ferric Salt of Triflimide Anions. *Energy Environ. Sci.* **2012**, *5* (11), 9639−9644.
(63) Noriega, R.; Rivnay, J.; Vandewal, K.; Koch, F. P. V.; Stingelin, N.; Smith, P.; Toney, M. F.; Salleo, A. A General Relationship between Disorder, Aggregation and Charge Transport in Conjugated Polymers. *Nat. Mater.* **2013**, *12* (11), 1038.
(64) Rivnay, J.; Inal, S.; Collins, B. A.; Sessolo, M.; Stavrinidou, E.; Strakosas, X.; Tassone, C.; Delongchamp, D. M.; Malliaras, G. G. Structural Control of Mixed Ionic and Electronic Transport in Conducting Polymers. *Nat. Commun.* **2016**, *7*, 11287.
(65) Menon, A. K.; Meek, O.; Eng, A. J.; Yee, S. K. Radial Thermoelectric Generator Fabricated from N- and P-Type Conducting Polymers. *J. Appl. Polym. Sci.* **2017**, *134* (3), 44060.
(66) Fang, H.; Popere, B. C.; Thomas, E. M.; Mai, C.-K.; Chang, W. B.; Bazan, G. C.; Chabinyc, M. L.; Segalman, R. A. Large-Scale Integration of Flexible Materials into Rolled and Corrugated Thermoelectric Modules. *J. Appl. Polym. Sci.* **2017**, *134* (3), 44208.
(67) Owoyele, O.; Ferguson, S.; O'Connor, B. T. Performance Analysis of a Thermoelectric Cooler with a Corrugated Architecture. *Appl. Energy* **2015**, *147* (SupplementC), 184−191.
(68) Hexemer, A.; Bras, W.; Glossinger, J.; Schaible, E.; Gann, E.; Kirian, R.; MacDowell, A.; Church, M.; Rude, B.; Padmore, H. A SAXS/WAXS/GISAXS Beamline with Multilayer Monochromator. *J. Phys. Conf. Ser.* **2010**, *247* (1), 012007.
(69) Hexemer, A.; Müller-Buschbaum, P. Advanced Grazing-Incidence Techniques for Modern Soft-Matter Materials Analysis. *IUCrJ* **2015**, *2* (1), 106−125.
(70) van Reenen, S.; Kemerink, M. Correcting for Contact Geometry in Seebeck Coefficient Measurements of Thin Film Devices. *Org. Electron.* **2014**, *15* (10), 2250−2255.

DOI: 10.1021/acs.chemmater.7b04849
Chem. Mater. 2018, 30, 998−1010